AIAA 80-1448R

Numerical Study of One-Dimensional Unsteady Particle-Laden Flows with Shocks

F. Marconi,* S. Rudman,* and V. Caliaf
Grumman Aerospace Corporation, Bethpage, N. Y.

A computational procedure for the prediction of one-dimensional unsteady gas/particle flows has been developed. It uses a characteristic based finite difference scheme, a fitted shock wave, and coordinate stretching. The mathematical nature of the gas/particle equations is developed and it is shown, for the first time, that they belong to a more general class of hyperbolic partial differential equations than the gas alone equations. Numerical results have been obtained for three shock tube flows: the propagation of a shock into infinite and finite particle clouds, and the reflection of a shock into a relaxation zone formed behind a shock wave propagating in an infinite particle cloud. The detailed time dependent development of these flows is shown and in the case of the infinite cloud the time asymptotic results are compared with computed steady results. The dependence of these shock tube flowfields on a number of parameters is studied.

Introduction

DURING the past twenty years shock-tube facilities have been applied to a broad range of two-phase flow problems with considerable success. The shock tube has been used in the determination of particle drag laws in gas particle systems,[1] heat and mass transfer in high-temperature particle laden gases,[2] the evaporation and ignition of liquid droplets,[3] kinetic data on the devolatilization of coal particles,[4] spectroscopic data required for the interpretation of astrophysical measurements,[5] and the establishment of a controlled infrared radiation data base for validation of rocket exhaust computer codes.[6] A detailed review of these and other applications may be found in Ref. 7. Shock-tube studies of aerosols usually are restricted to those cases where the aerosol flow can be considered steady in shock-fixed coordinates; i.e., quasisteady or time asymptotic solutions give aerosol properties. In this paper a numerical calculation procedure is presented that permits calculation of the time-dependent properties of particle laden gases that have been shock processed. The developed code will permit investigations of unsteady aerosol flows and should also permit an extended operational range for shock tube investigations where the aerosol clouds are of finite extent.[6,8,9]

Two-phase gas/solid particle flows are fluid dynamics problems that have thermal and momentum relaxation phenomena. In the continuum view the two-phase medium appears to have sources (or sinks) of momentum and energy that are distributed throughout. The nature and extent to which particles influence a fluid flow is determined by the relative magnitudes of the relaxation time of the particles and the fluid element transit time. Any discontinuous or rapid change in gas properties is followed by a relaxation zone in which the gas and particles come to equilibrium; this is the situation with a shock propagating in a shock tube. The structure of the shock wave/relaxation zone has been investigated by a number of authors[10-12] for fully developed or equilibrium flows. These studies employ shock-fixed coordinates transforming the problem into a steady one. The temporal development of the flow, the influence of cloud boundaries or end walls can not be achieved by these type analyses. These effects can only be incorporated by the solution of the unsteady flow equations.

This paper presents both theoretical and numerical developments of interest in gas/particle studies. On the theoretical side, the nature of the particle equations has been elucidated for the first time. The form of the particle equations precludes combining them in the usual characteristic form. It is shown that these equations are actually a more general form of hyperbolic equation than is normally encountered in pure gas flows. Solutions of these equations indicate the necessary properties that a sound computational scheme must employ (e.g., characteristic direction, domains of dependence, etc.). On the numerical side, the characteristic based finite-difference scheme presented by Moretti[13] has been applied to the study of one-dimensional unsteady particle laden flows. An exponential stretching of grid points is required in order to resolve the relaxation zone behind the shock. In the case of a finite cloud, the cloud boundaries are followed explicitly. In all the computations of the present study, a fitted discontinuous shock front satisfying the frozen particle Rankine-Hugoniot jump conditions is employed.

In the following sections of this paper, the computational procedure used in this work is outlined briefly, the mathematical analysis of the governing equations is discussed, and numerical results are presented for three classes of shock tube flows; shock wave propagation into infinite and finite aerosol clouds, and the reflection of a shock into a relaxing aerosol cloud. In the case of an incident shock in an infinite gas/particle cloud the time asymptotic results are compared with those of a steady (shock-fixed) computation. The effects of particle loading, particle size, and shock Mach number on the shock relaxation zone structure and temporal development of the flow from an impulsive start are studied in detail. In the case of a reflected shock into a relaxing aerosol the effect of initial shock Mach number is studied and, finally, in the case of a finite cloud the effect of cloud extent is studied.

Analysis and Numerical Technique

The gas/particle aerosols considered in this paper are limited by the following assumptions. The gas is calorically and thermally perfect, and its viscosity and thermal conductivity are constant. The particles are incompressible, spherical, and uniform in size. The specific heat is constant and the temperature is uniform within each particle. The particles do not interact with each other and do not contribute

Presented as Paper 80-1448 at the AIAA 13th Fluid and Plasma Dynamics Conference, Snowmass, Colo., July 14-16, 1980; submitted July 24, 1980; revision received April 20, 1981.

*Senior Staff Scientist, Research Department. Member AIAA.
†Staff Scientist, Research Department.

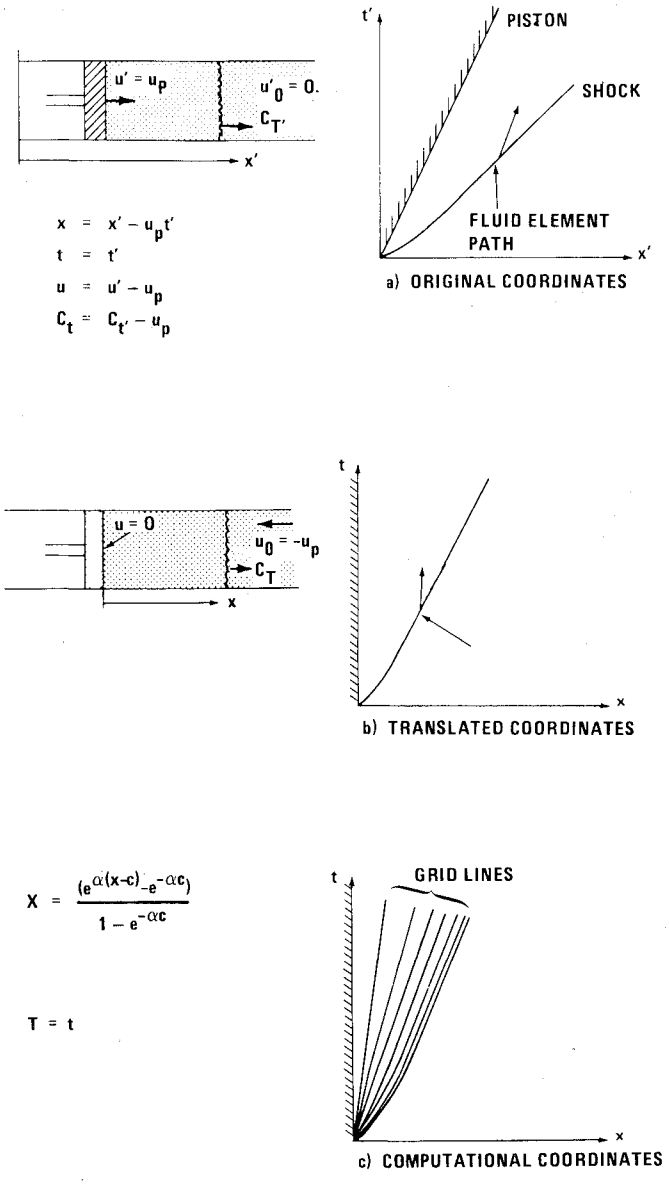

Fig. 1 Schematic of coordinate systems.

to the pressure. The particle size is assumed small compared to the shock-tube diameter so that the mixing in each particle's wake is assumed to occur instantaneously. The particles are uniformly distributed transversely over the constant cross section of the shock tube, so that the flow is one dimensional. Boundary-layer effects and heat exchange with walls are neglected. However, the viscosity and thermal conductivity of the gas are considered in producing particle drag and heat transfer between the gas and particle. The drag coefficient and Nusselt number are assumed to be prescribed functions of local particle Reynolds number. When particles interact with an end wall of the tube (or the driving piston), they are assumed to stick to the surface. The particle relaxation time is long enough so that they pass through the shock unaffected. No external forces (such as gravity) or external heat exchange affect the mixture. Finally, no mass transfer is considered between the solid and gas phases.

The coordinate system used in the present work is shown in Fig. 1 where u is the gas velocity, C_t the shock speed, u_p the piston velocity, and the subscript 0 indicates undisturbed conditions. In the translated coordinate (Fig. 1b) the piston is always at $x=0$ and the boundary condition at the piston is $u=0$. In the case of the shock reflection from the shock-tube end wall, the coordinate system is fixed at the end wall (again the boundary condition becomes $u=0$). The computational plane coordinates X, T are defined by the expressions in Fig. 1c. In the expression for $X(x,t)$, C is the shock position at any time. The transformation normalizes the spatial coordinate x so that the piston ($x=0$) is at $X=0$ and the shock ($x=C$) is at $X=1$. In addition, the transformation forces the evenly distributed mesh points in the X, T plane to be concentrated near the shock in the physical (x,t) plane (Fig. 1c). Based on the analysis of Marble[14] α is chosen so that the relaxation zone behind the shock has a sufficient number of grid points for all time.

Using the notation of Rudinger[12] the equations governing the gas phase are the compatibility equations along the $u \pm a$ characteristics

$$\frac{\delta^+ P}{\delta t} = \frac{a}{\gamma R}\frac{\delta^+ S}{\delta t} + \frac{\gamma - 1}{\gamma R} a\zeta - \frac{\sigma}{\rho}\phi \tag{1}$$

$$\frac{\delta^- Q}{\delta t} = \frac{a}{\gamma R}\frac{\delta^- S}{\delta t} + \frac{\gamma - 1}{\gamma R} a\zeta - \frac{\sigma}{\rho}\phi \tag{2}$$

and the energy equation

$$\frac{DS}{Dt} = \frac{\sigma}{\rho}\frac{\gamma R}{a^2}[(u-v)\phi - c\psi] = \zeta \tag{3}$$

$$\frac{\delta^\pm}{\delta t} = \frac{\partial}{\partial t} + (u \pm a)\frac{\partial}{\partial x}, \qquad \frac{D}{Dt} = \frac{\partial}{\partial t} + u\frac{\partial}{\partial x}$$

are the derivatives along the $dx/dt = u \pm a$ and u, respectively. The dependent variables are the Riemann variable $P = u + 2a/(\gamma - 1)$ and $Q = u - 2a/(\gamma - 1)$; u, a, S, and ρ are the gas velocity, speed of sound, entropy, and density. γ and R are the ratio of specific heats and gas constant. σ, v, and τ are the particle density, velocity, and temperature. The terms, ϕ and ψ are the drag forces and heat transfer between the particles, and the gas

$$\phi = C_D 3\rho \mid u - v \mid (u-v)/4D\rho_p, \quad \psi = 6kNu(T-\tau)/\rho_p c D^2$$

where C_D and Nu are the drag coefficient and Nusselt numbers, and D, ρ_p, c, and k are the particle diameter, solid phase density, solid phase specific heat, and gas thermal conductivity, respectively.

For the particles the equations of mass, momentum, and energy conservation are

$$\frac{D_p \sigma}{Dt} = -\sigma\frac{\partial v}{\partial x} \tag{4}$$

$$\frac{D_p v}{Dt} = \phi \tag{5}$$

$$\frac{D_p \tau}{Dt} = \psi \tag{6}$$

where the derivative $D_p/Dt = \partial/\partial t + v\partial/\partial x$ is the derivative along the particle path, the fourth characteristic of the set of governing equations. Equations (1-6) represent a set of six equations for the six primary unknowns u, a, S, σ, v, and τ (u and a are related to the Riemann invariants simply). The coefficients of Eqs. (1-6) are evaluated employing the gas equation of state and speed of sound

$$T = a^2/\gamma R \qquad \rho/\rho_0 = \exp\left\{\frac{1}{\gamma - 1}\ln\frac{T}{T_0} - \frac{S - S_0}{R}\right\} \tag{7}$$

In the present work the widely used drag coefficient due to Gilbert et al.[15] and Nusselt number of Knudsen and Katz[16]

are employed. These formulas may introduce errors because they do not include compressibility or rarefaction corrections.

$$C_D = 28R_e^{-0.85} + 0.48 \qquad Nu = 2 + 0.6P_r^{1/3}\sqrt{Re} \tag{8}$$

Pr is the gas Prandtl number, Re (the single particle Reynolds number) $= |u-v|\rho D/\mu$, and μ is the gas viscosity.

The finite difference algorithm developed by Moretti[13] is employed in the present work. This scheme is based upon using characteristic directions to determine the form of spatial differences. This finite difference scheme requires that the governing equations be employed in standard characteristic form. The scheme must satisfy the standard Courant, Friedricks, Lewy (CFL) condition for stability. The presence of particles introduces a fourth characteristic (particle path) to be considered in the CFL condition. The coordinate stretching which had to be used in the relaxation zone reduces the marching step significantly via the CFL condition. The gas Eqs. (1-3) are in proper characteristic form. The particle equations cannot be reduced to this form.[17-19] In the following discussion this dilemma is resolved by recognizing that these equations belong to a more general class of hyperbolic equation.

The particle temperature equation (6) is already in characteristic form (slope, $\dot{x}=v$) and is not included in the following discussion. Using matrix notation, Eqs. (4) and (5) are

$$U_t + AU_x = B \tag{9}$$

where

$$U = \begin{bmatrix} v \\ \Sigma \end{bmatrix}, \quad A = \begin{bmatrix} v & 0 \\ 1 & v \end{bmatrix}, \quad B = \begin{bmatrix} \phi \\ 0 \end{bmatrix}$$

and $\Sigma = \ell n\sigma$.

The matrix A has two real eigenvalues ($\lambda_{1,2} = v$) but cannot be diagonalized since it is already in Jordan Canonical form. If A could be diagonalized then the set of Eqs. (9) could be reduced to a set of uncoupled scalar equations which are the compatibility conditions along the characteristics.[20] The nature of the solution of Eqs. (9) can be studied by solving Eqs. (9) for constant coefficient matrix A. With initial conditions

$$U = U_0(x) = \begin{bmatrix} v_0(x) \\ \Sigma_0(x) \end{bmatrix}$$

The solution is

$$U = \begin{bmatrix} v_0(x-\lambda t) + t\phi \\ \Sigma_0(x-\lambda t) - tv_0'(x-\lambda t) \end{bmatrix} \tag{10}$$

The solution was found by considering the equations in scalar form, introducing characteristic coordinates, and integrating the two equations sequentially. More details are to be found in Ref. 21. The solution for v is identical to that of an ordinary hyperbolic equation. It is a combination of a homogeneous solution $[v_0(x-\lambda t)]$ which represents a wave that propagates the initial conditions along the lines $\dot{x}=\lambda$, and a particular solution which accounts for the forcing term ϕ. The solution for Σ is identical in form except that the term $-v_0'(x-\lambda t)$ replaces ϕ. Therefore, the effect of having a Jordan coefficient matrix is to introduce a term in the solution in much the same way that a forcing term would appear. The term, however, is the derivative of the complimentary variable and is evaluated along the characteristic $x-\lambda t$.

The properties of the solution are very much similar to that of any ordinary hyperbolic system. Only a single value can be specified on each characteristic line determining the solution for all later times. The initial functions $v_0(x)$ and $\Sigma_0(x)$ serve to set these values. Therefore, when a particle path intersects an end wall or a piston that have specified velocities, an auxiliary condition must be specified. In all the calculations in the present analysis the particles are considered to adhere to the piston. Since the solution Eq. (10) is the same in nature as an ordinary hyperbolic system, we use the same differencing in the λ scheme as with the other equations [(1-3) and (6)]. The term $-\partial v/\partial x$ that appears on the right-hand side of Eq. (4) is differenced in the biased manner of the λ scheme because in the solution Eq. (10) it appears along the characteristic. All aspects of the computational techniques used in the present work are presented in more detail in Ref. 21.

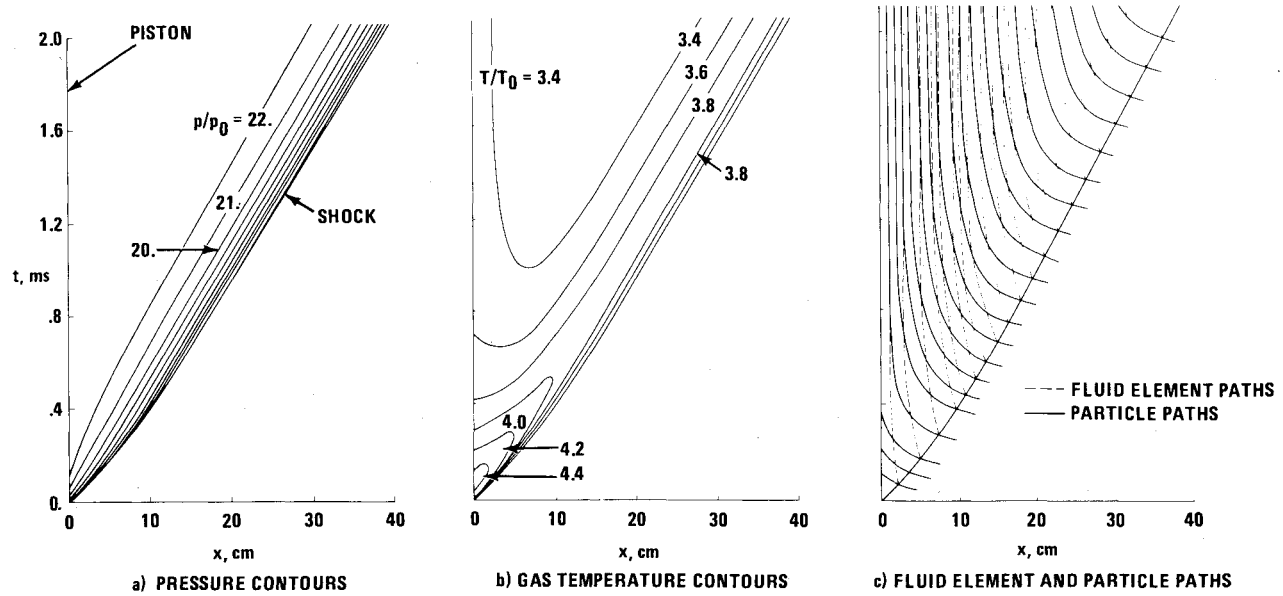

Fig. 2 Development of the flowfield, piston generated shock propagating into an infinite particle cloud; 10 μm aluminum oxide particles, $u_p/a_0 = 3$, $\sigma_0/\rho_0 = 0.5$.

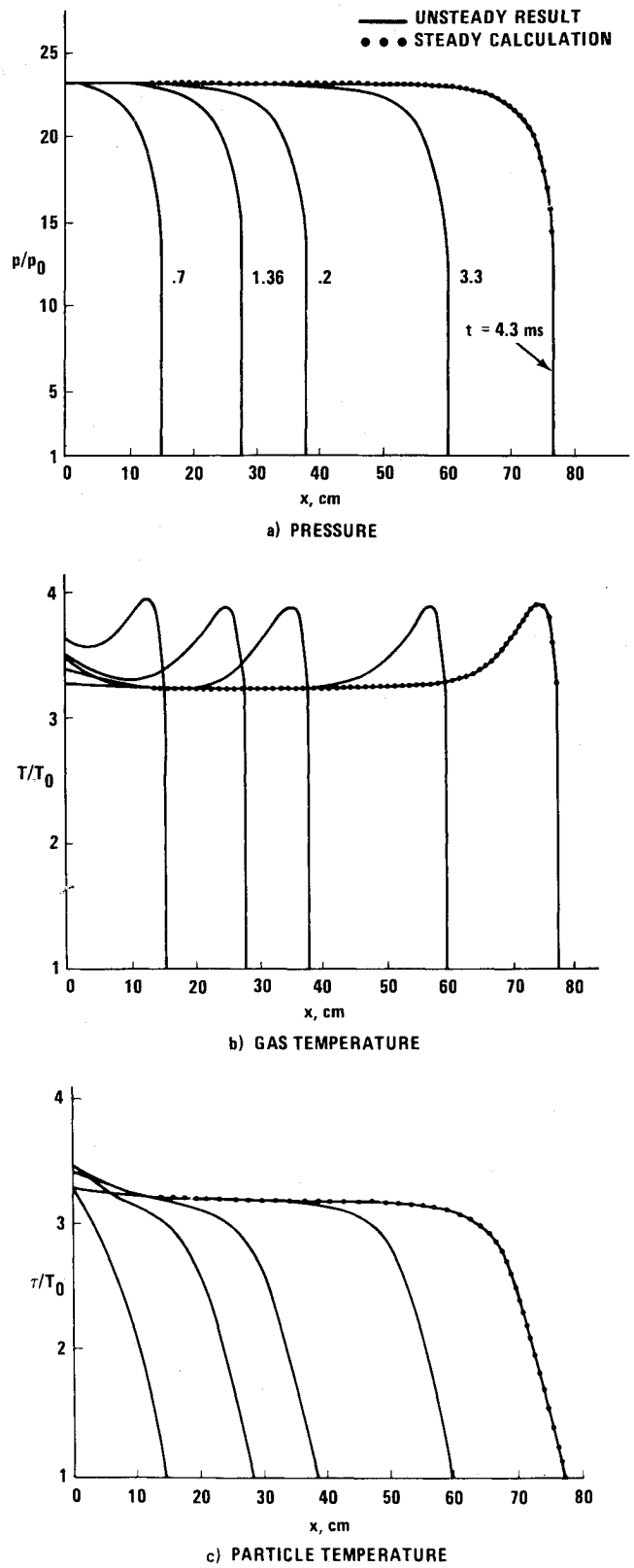

Fig. 3 Spatial distributions of gas and particle properties at several times; 10 μm aluminum oxide particles, $u_p/a_0 = 3$, $\sigma_0/\rho_0 = 0.5$.

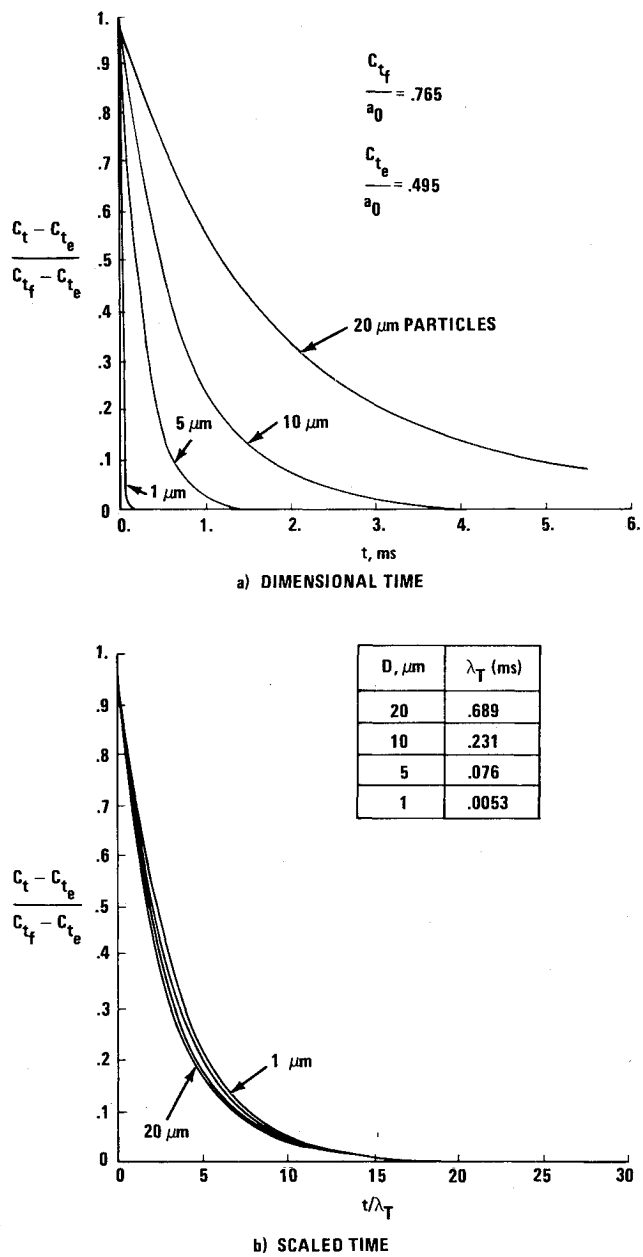

Fig. 4 Shock decay vs time for several particle sizes; $u_P/a_0 = 1$, $\sigma_0/\rho_0 = 0.5$.

Discussion of Results

The numerical procedure developed in this paper has been used to analyze several cases of shock-processed particle clouds to illustrate its application. Three cases are considered: 1) a shock propagating into an infinitely long, uniformly loaded particle cloud; 2) the reflection of a shock wave from a solid boundary into the relaxation zone formed behind the incident shock of case 1; and 3) the propagation of a shock into a finite length, uniformly loaded particle cloud. In all cases studied the test gas is air and the particles are aluminum oxide. The relevant particle properties are the particle density $\rho_p = 4$ g/cm^3 and specific heat $c = 1.25 \times 10^7$ cm^2/s^2 K. The piston velocity u_p, particle diameter D, and the concentration ratio of the particles to gas σ_0/ρ_0 are treated as variables in each case studied after first establishing base line results with u_p, D and σ_0/ρ_0 of $3a_0$, 10 μm, and 0.5, respectively. The results are presented in the translated coordinate system illustrated in Fig. 1b.

In case 1 the flowfield is established at $t = 0$ by impulsively accelerating a piston to constant velocity. In front of the piston a shock is formed immediately which accelerates to the speed required to produce a gas velocity equal to the piston velocity. Figure 2 shows the development of the flow in the x-t contour plots of pressure (Fig. 2a) and gas temperature (Fig. 2b). The particle and fluid element paths are shown in Fig. 2c. The piston velocity in this case is quite large ($u_p = 3a_0$) indicating a strong shock. The relaxation zone in pressure and temperature, as indicated by the closely spaced contour lines running parallel to the shock, is "steady" relative to the shock

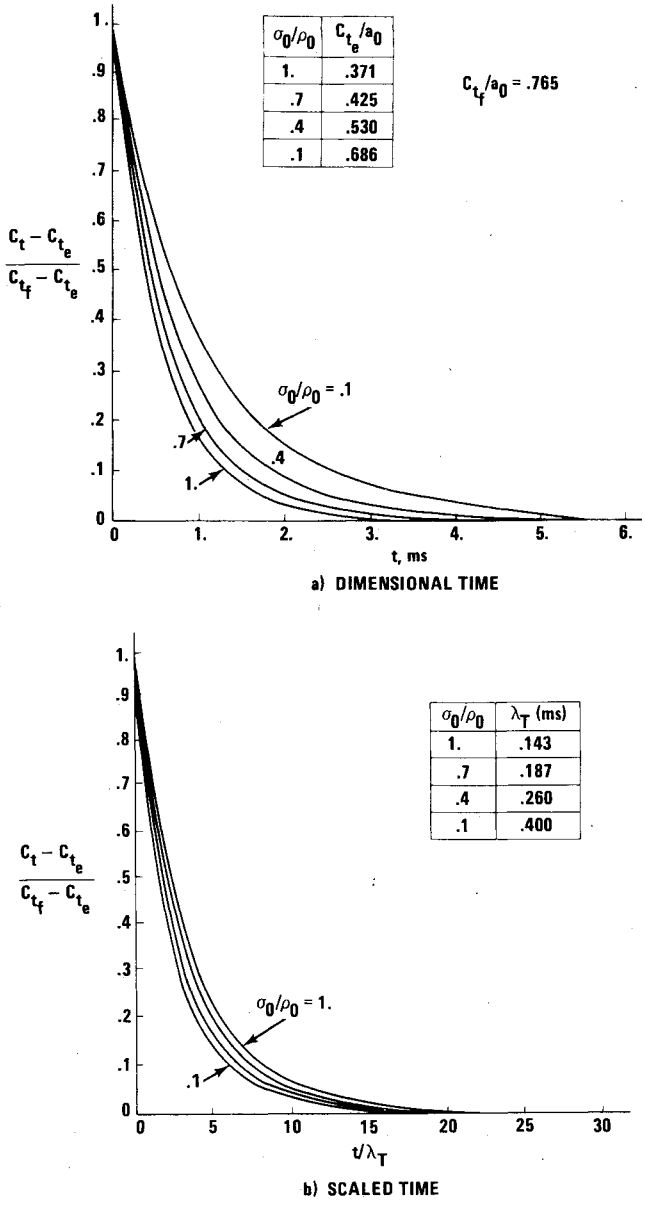

Fig. 5 Shock decay vs time for several particle mass loadings; $u_P/a_0 = 1$, 10 μm particles.

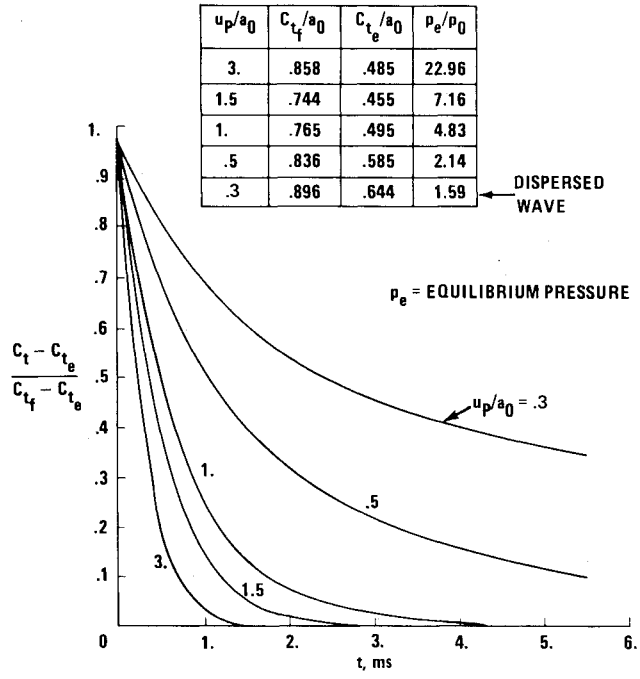

Fig. 6 Shock decay vs time for several piston speeds (shock strengths); 10 μm particles, $\sigma_0/\rho_0 = 0.5$.

front for times greater than 1.2 ms. The equilibrium pressure ratio for this case is 22.96 and is established in a region behind the last isobar of Fig. 2a. The temperature relaxation zone is longer than that of the pressure, as is true of all the cases studied in this work. The equilibrium temperature ratio is 3.201 and is established in the zone between the $T/T_0 = 3.4$ contours (not shown in figure, see Fig. 3) at a time after 1.6 ms. There is a region close to the piston in which the temperature never reaches its equilibrium value. This is because the particle and fluid elements that pass through the equilibrium shock (Fig. 2c) never reach the piston. This effect is analogous to the entropy layer close to a two-dimensional blunt body. Figure 2c shows how the particles slip relative to the gas and finally reach the gas velocity.

In Fig. 3, the spatial distribution of gas and particle properties at several times in the development of the flow shown in Fig. 2 is presented. For the last time shown in each figure ($t = 4.3$ ms) the results are compared with calculations that are obtained from a steady-state (shock-fixed) analysis. The two results are virtually identical, indicating that the unsteady flow has reached a steady state relative to the shock front. This comparison also serves to check the unsteady computational scheme against the well-established steady counterpart. The layer near the piston can be seen in the variation of all quantities which are transmitted along particle and fluid element paths (gas and particle temperatures T and τ). The overshoot in gas temperature immediately behind the shock front (Fig. 3b) is due to the heating of the gas as the particles are decelerated rapidly just behind the shock. After this peak the gas is cooled as it approaches equilibrium with the particles.

Figures 4-6 present the results of a study of the transient shock velocities for an impulsively started flow. A piston generated shock propagating into an infinite particle cloud starts moving at its frozen speed (C_{tf}, pure gas shock speed) as the piston is impulsively accelerated. As the flow develops the shock slows down and eventually attains an equilibrium shock speed (C_{te}, equivalent pseudo gas shock speed) that is lower than that of the pure gas shock speed. Figure 4a shows the shock decay vs time for various sized particles and indicates a more rapid approach to equilibrium for decreasing particle size. Figure 4b is a plot of the same cases, with the time scale normalized with respect to the temperature relaxation time predicted by the analysis of Marble.[14]

$$\lambda_T = \Lambda_T \Big/ \left[1 + \frac{c/c_p\,(\sigma_0/\rho_0)}{1 - M^2}\right] \sqrt{p_0/\rho_0}$$

Λ_T is the relaxation length associated with a single particle while λ_T is a gas/particle system relaxation time and not that associated with a single particle. It is evident from Fig. 4b that λ_T has the proper dependence on particle size.

Figure 5a shows the shock decay for several particle mass loadings. It can be seen from the figure that the shock decays more quickly for the heavier loading. Figure 5b shows these results reduced with the relaxation time λ_T. Here again the parameter λ_T appears to be a good time scale for the problem.

Figure 6 shows the shock decay for several piston velocities or (equivalently) shock strengths. The shock speed approaches its equilibrium value more slowly for the weaker shocks. This is because the equilibration of the flow requires communication between the piston and the shock through characteristic waves (in parallel with the relaxation process of the particles). In the weak shock cases the equilibrium shock speed and the local sound speed are nearly the same so that the

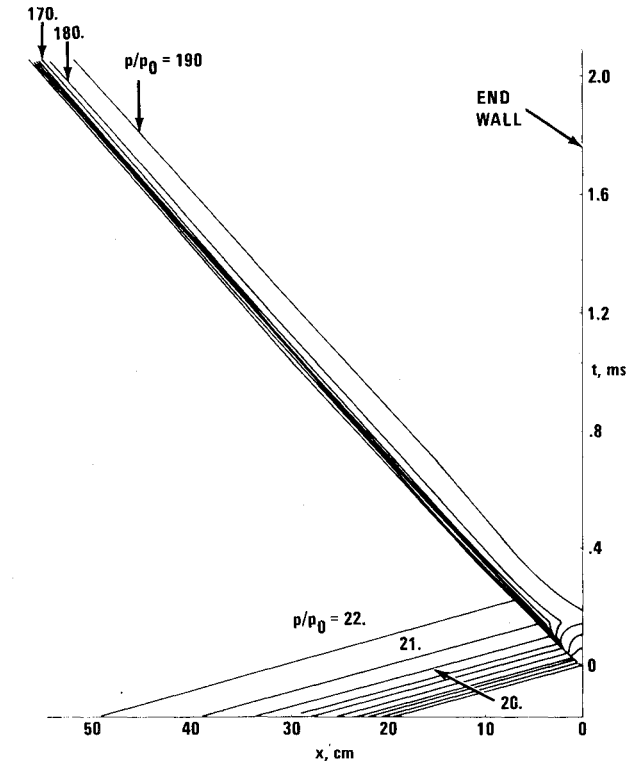

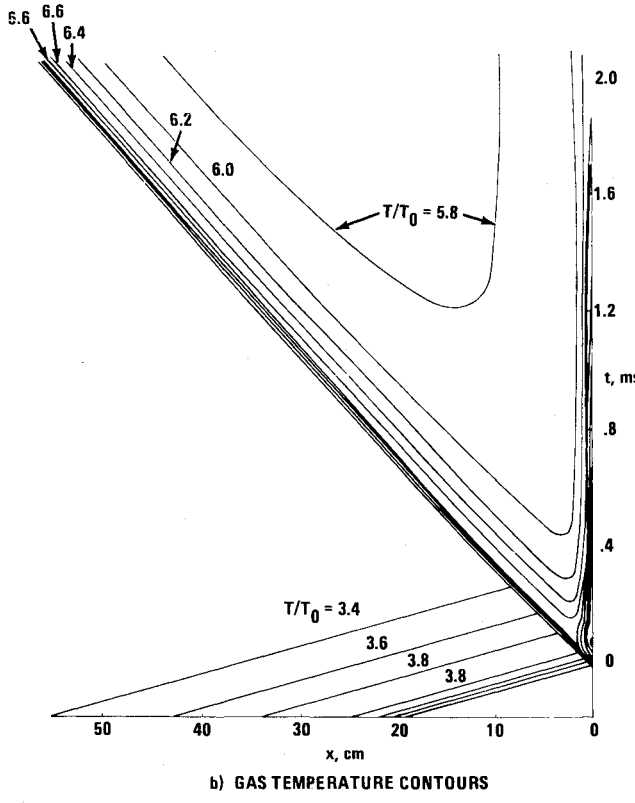

Fig. 7 Development of the flowfield, reflected shock into relaxation zone, infinite particle cloud; 10 μm aluminum oxide particles, $u_p/a_0 = 3$, $\sigma_0/\rho_0 = 0.5$.

characteristics require a much longer time to travel from the piston to the shock. In the weakest case shown in Fig. 6 ($u_p/a_0 = 0.3$) the shock never reaches the equilibrium wave speed but instead asymptotes to the local undisturbed frozen speed of sound. This dispersed wave develops because the equilibrium Mach number relative to the front is supersonic while the frozen counterpart is subsonic.[12] The parameter λ_T

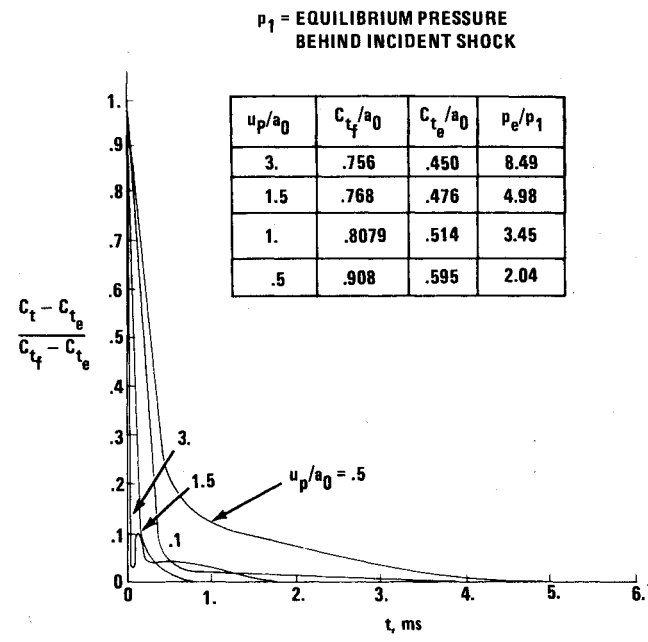

Fig. 8 Shock decay vs time, reflected shock, for several piston velocities; $D = 10\ \mu$m, $\sigma_0/\rho_0 = 0.5$.

did not reduce this data well because it does not account for the acoustic process.

Case 2 is the flow generated by a shock reflecting from an end wall into the relaxation zone it has previously formed. The initial condition for this flowfield are: the reflected shock starts at its frozen shock speed slightly away from the end wall and propagates into the relaxation zone behind the incident shock. The distribution of gas/particle properties on the low pressure side of the shock is computed with the steady-state code and consists of a relaxation zone followed by the constant equilibrium conditions of the incident shock. The initial gas/particle properties and the incident shock strength corresponds to that of Fig. 2. Figure 7 shows an initial transient after which the flow develops a relaxation zone and constant equilibrium region. The equilibrium pressure $p_e/p_0 = 195$ is established just behind the last contour shown in Fig. 7a where p_0 is the undisturbed pressure in front of the incident shock. The equilibrium temperature $T_e/T_0 = 5.75$ is established in a region between the shock and the end wall in the region between the $T/T_0 = 5.8$ contours of Fig. 7b. Figure 7b shows the same kind of entropy layer region near the end wall that was shown near the piston in the results of Fig. 2b. Figure 7 shows that the relaxation zone behind the reflected shock is shorter than that behind the incident shock. This results because the density upstream of the reflected shock is seven times higher. For the same reason the reflected shock reaches its equilibrium velocity in a shorter time than the incident shock. Figure 8 shows the reflected shock decay for several piston velocities (the conditions are the same as the incident shocks of Fig. 6). It is interesting to note that the reflected shocks do not all decay monotonically as did the incident shocks. The effect is evident for $u_p/a_0 = 3$ and diminishes as u_p decreases to $u_p/a_0 = 0.5$. This effect is due to the temperature overshoot in the relaxation zone behind the incident shock (Fig. 3b) which diminishes at smaller u_p/a_0, and does not exist at $u_p/a_0 = 0.5$.

The final problem considered is that of a piston generated shock propagating through a finite particle cloud. In these flowfields, the particle cloud is initially a given distance from the piston, all gas and particle properties are uniform. The shock moves at its frozen speed into a pure gas until it encounters the leading edge of the cloud, Fig. 9. Once the shock reaches the cloud it begins to slow down in a manner similar to the case of an infinite cloud. Figure 9a shows the isobars.

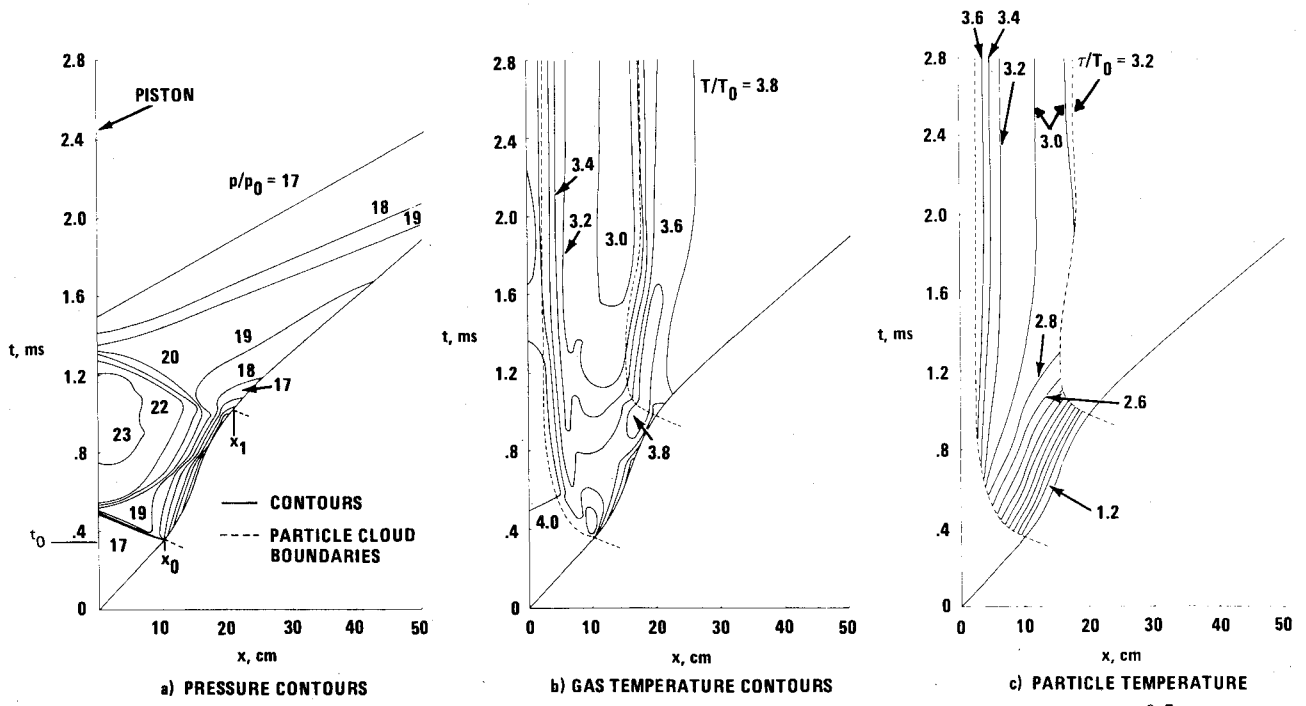

Fig. 9 Development of the flowfield, finite particle cloud; 10 μm aluminum oxide particles, $u_p/a_0 = 3$, $\sigma_0/\rho_0 = 0.5$.

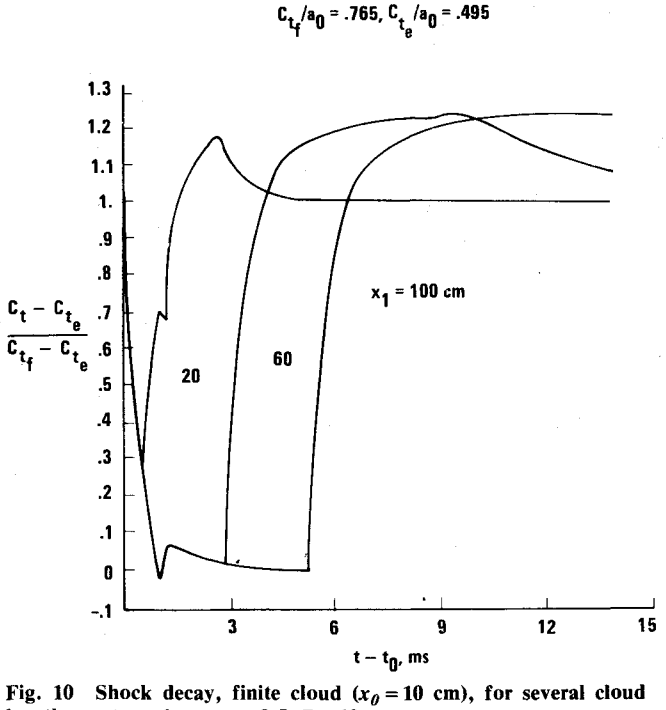

Fig. 10 Shock decay, finite cloud ($x_0 = 10$ cm), for several cloud lengths; $u_p/a_0 = 1$, $\sigma_0/\rho_0 = 0.5$, $D = 10$ μm.

The wave patterns for this flowfield are much more complex than those for the incident or reflected shocks in an infinite cloud. Reflected waves are generated when the shock wave enters and leaves the cloud. A compression is sent toward the piston when the shock first encounters the cloud. The same type of compression occurred in all the strong shock flows ($u_p/a_0 = 3$) shown in this work, but they occurred so close to the piston or end wall in the case of the infinite cloud that they do not show up on the time scales used in Figs. 2a and 7a. After the shock leaves the particle cloud it eventually returns to its initial frozen speed as it propagates in a pure gas again. The pressure behind the shock becomes constant at its initial frozen value ($p_f/p_0 = 17.2$), and the gas and particles both come to rest relative to the piston. Figures 9b and 9c show the gas and particle temperature distributions. For times greater than 2 ms the flowfield within the cloud is steady and local gas/particle thermal equilibrium has been established. A small region of constant uniform temperature has been established ($T = 3.0T_0$) but this temperature does not correspond to the pseudo gas equilibrium value of $3.2T_0$. For longer clouds the pseudo gas equilibrium value is obtained (see discussion following). Outside the cloud, between the cloud boundary and the shock, the gas temperature approaches its constant frozen value, $T_f = 3.8T_0$, at approximately 3 ms.

Figure 10 shows the shock speed decay for several cloud lengths (x_0, x_1, t_0 are defined in Fig. 9a). The shock decreases in speed as it first encounters the cloud ($t - t_0 = 0$), and picks up speed as it emerges from the cloud. The shock speed overshoots its frozen value and finally asymptotes to it slowly. For the three cases shown the change in shock speed at 1.12 ms is due to waves generated when the cloud is first encountered, which reflect from the piston and overtake the shock at $t - t_0 = 1.12$ ms. It is evident from Fig. 10 that the pseudo gas equilibrium condition is established if the cloud is long enough; i.e., equilibrium shock speed is obtained within the cloud.

Conclusions

The mathematical nature of the equations which govern particle laden flows was analyzed and it is shown that they belong to a more general class of hyperbolic partial-differential equation than those of the gas alone. An efficient characteristic-based finite-difference technique was developed based on this analysis. The resulting computational procedure was used to make a detailed study of these flowfields. Several illustrative examples were considered that demonstrate the overall utility of the code. In the first case studied, the time dependent development of the flowfield behind a shock propagating into an infinite cloud was shown in detail. The solutions for the shock speed were shown to correlate reasonably well using a time scale based on a linear analysis of the equations. The sensitivity of the shock wave variation to particle size, initial particle to gas concentration ratio, and the frozen shock strength was elucidated for the first time. The unsteady numerical computations were checked by comparison with equilibrium solutions. In the second case studied

the ability to treat a shock wave interacting with a nonequilibrium particle cloud was illustrated by considering the reflection of a shock front from an end wall into the relaxation zone following the incident shock wave. Finally, the propagation of a shock into a finite length uniformly loaded particle cloud was considered because this is a reasonable model for many experimental shock-tube configurations. The case of a shock incident on uniformly loaded finite clouds of several different lengths was considered. It was noted that the magnitude of the equilibrium properties could be described adequately by the pseudo gas analysis if the cloud extent was sufficiently large relative to the shock-wave relaxation lengths. In these cases where the clouds are too short experiments are still possible if the unsteady calculations are used to predict the test section properties.

References

[1] Rudinger, G., "Effective Drag Coefficients for Gas-Particle Flow in Shock Tubes," Project SQUID Technical Rept. CAL-97-PU, March 1969.

[2] Nettleton, M. A., "Heat Transfer to Particles in Shock Heated Gases," *AIAA Journal,* Vol. 4, May 1966, p. 939.

[3] Mullaney, G. J., "Shock Tube Technique for Study of Auto Ignition of Liquid Fuel Sprays," *Industrial and Engineering Chemistry,* Vol. 50, Jan. 1958, p. 53.

[4] Lowenstein, A. I. and von Rosenberg, C. W. Jr., "Shock Tube Studies of Coal Devolatilization," *Shock Tube and Shock Wave Research, Proceedings of 11th International Symposium on Shock Tubes and Waves,* Seattle, July 1977, pp. 11-14.

[5] Nicholls, R. W., Parkinson, W. H., and Reeves, E. M., "The Spectroscopy of Shock-Excited Powdered Solids," *Applied Optics,* Vol. 2, Sept. 1963, p. 919.

[6] Oman, R. A., Konopka, W., and Calia, V. S., "A Technique for Controlled Gas/Particle Radiation Experiments," Grumman Aerospace Corp., Bethpage, N. Y., Research Dept. Memo. RM-686J, April 1979.

[7] Nettleton, M. A., "Shock Wave Chemistry in Dusty Gases and Fogs: A Review," *Combustion and Flame,* Vol. 28, 1977, pp. 3-16.

[8] Mirtich, M. J. and Herman, M., "Feasibility of Accelerating Micron-Size Particles in Shock Tube Flows for Hypervelocity Degradation of Reflective Surfaces," NASA TND-3187, Jan. 1966.

[9] Nettleton, M. A. and Stirling, R., "The Ignition of Clouds of Particles in Shock Heated Oxygen," *Proceedings of the Royal Society,* Vol. A300, 1967, p. 62.

[10] Carrier, G. F., "Shock Waves in a Dusty Gas," *Journal of Fluid Mechanics,* Vol. 4, March 1958, pp. 376-383.

[11] Marble, F. E., "Dynamics of a Gas Containing Small Solid Particles," *5th AGARD Colloquium on Combustion and Propulsion; High Temperature Phenomena,* Braunschwerg, April 9-13, 1962, Pergamon Press, New York, 1962, pp. 175-215.

[12] Rudinger, G., "Relaxation in Gas Particle Flow," *Nonequilibrium Flows,* edited by P. P. Wegener, Vol. 1, Marcel Dekker, New York, Chap. 3, Pt. 1, pp. 119-161.

[13] Moretti, G., "The λ-Scheme," *Computers and Fluids,* Vol. 7, 1979, pp. 191-205.

[14] Marble, F. E., "Dynamics of Dusty Gases," *Annual Review of Fluid Mechanics,* Vol. 2, Annual Reviews Inc., 1970, pp. 397-446.

[15] Gilbert, M., Davis, L., and Altman, D., "Velocity Lag of Particles in Linearly Accelerated Combustion Cases," *Jet Propulsion,* Vol. 25, 1955, pp. 26-30.

[16] Knudsen, J. G. and Katz, D. L., *Fluid Mechanics and Heat Transfer,* McGraw Hill, New York, 1958, p. 511.

[17] Outa, E., Tajima, K., and Morii, H., "Experiments and Analyses on Shock Waves Propagating through a Gas Particle Mixture," *Bulletin of Japanese Society of Mechanical Engineers,* Vol. 19, April 1978, pp. 384-394.

[18] Sauerwein, H. and Fendell, F., "Method of Characteristics in Two Phase Flow," *Physics of Fluids,* Aug. 1965, pp. 1564-1565.

[19] Migdal, D. and Agosta, V. D., "A Source Flow Model for Continuum Gas Particle Flow," *Journal of Applied Mechanics,* Vol. 34, 1967, pp. 860-865.

[20] Kreiss, H. O., "Numerical Methods for Hyperbolic Partial Differential Equations," *Numerical Methods for Partial Differential Equations,* edited by S. V. Parter, Academic Press, New York, 1979.

[21] Marconi, F., Rudman, S., and Calia, V., "One Dimensional Unsteady Two Phase Flows with Shock Waves," AIAA Paper 80-1448, 1980.